A numerical model for the coupled long-term evolution of salt marshes and tidal flats

Giulio Mariotti[1] and Sergio Fagherazzi[1]

[1]   A one-dimensional numerical model for the coupled long-term evolution of salt marshes and tidal flats is presented. The model framework includes tidal currents, wind waves, sediment erosion, and deposition, as well as the effect of vegetation on sediment dynamics. The model is used to explore the evolution of the marsh boundary under different scenarios of sediment supply and sea level rise. Numerical results show that vegetation determines the rate of marsh progradation and regression and plays a critical role in the redistribution of sediments within the intertidal area. Simulations indicate that the scarp between salt marsh and tidal flat is a distinctive feature of marsh retreat. For a given sediment supply the marsh can prograde or erode as a function of sea level rise. A low rate of sea level rise reduces the depth of the tidal flat increasing wave dissipation. Sediment deposition is thus favored, and the marsh boundary prograde. A high rate of sea level rise leads to a deeper tidal flat and therefore higher waves that erode the marsh boundary, leading to erosion. When the rate of sea level rise is too high the entire marsh drowns and is transformed into a tidal flat.

1.   Introduction

[2]   Intertidal salt marshes are among the richest ecosystems in terms of productivity and species diversity, providing habitat to a diverse fauna population, important resources for fishing and recreation, and a storm buffer at the land-sea interface [*Allen*, 2000; *Fagherazzi et al.*, 2004]. Salt marshes are increasingly threatened by sea level rise, variations in storm activity, and land use. The extension of marshes in shallow coastlines is controlled by the repartition of sediments between tidal flats and marsh platform, and by the dynamics of the marsh boundary [*van de Koppel et al.*, 2005]. As a results salt marshes coevolve with tidal flats in the intertidal area [*Fagherazzi et al.*, 2006], and only a holistic approach encompassing the two landforms as well as the feedbacks between morphodynamics and ecology can determine the future trajectory of the system.

[3]   The processes that control sediment mobility are primarily physical: erosion, transportation and deposition induced by purely hydrodynamic forcing, like tidal currents and wind waves [see *Fagherazzi et al.*, 2007]. However, often biota interacts with sediment dynamics, strongly affecting the morphology of intertidal landscapes [*Le Hir et al.*, 2007].

[4]   Physical and biological processes are nonlinear and tightly coupled. Marsh elevation [*Morris et al.*, 2002], as well

as wave exposure [*van de Koppel et al.*, 2005], influence vegetation growth. Plants regulate sediment erodibility and trapping [*Le Hir et al.*, 2007], organogenic production [*Blum and Christian*, 2004], and wave dissipation [*Möller*, 2006]. These feedbacks produce complex dynamics in the coupled marsh−tidal flat evolution. One emergent feature from these dynamics is a vertical scarp separating salt marshes and tidal flats. Once the scarp is formed, local erosional processes such as piping, sapping, and bank failure take place, modifying the rate of marsh regression and ultimately the total extension of marsh surfaces along the coastline.

[5]   Several numerical models for the evolution of intertidal landforms have been proposed in the recent past. *Pritchard et al.* [2002] developed a cross-shore mudflat model that takes into account tidal effects; *Waeles et al.* [2004] incorporated in the same framework wind waves. *Le Hir et al.* [2007] focused on the effect of vegetation, introducing mud strengthening by microphytobenthos and hydrodynamic damping by salt marshes. All these models utilize a very large spatial grid (elements larger than 100 m), which is suitable to study the large-scale profile of tidal flats, but it does not permit the description of local features, like a vertical scarp, whose horizontal characteristic length scale is on the order of meters. In recent years, a new generation of models coupling biology to morphodynamics has been developed for intertidal areas [*Mudd et al.*, 2004]. For example, the model proposed by *Kirwan and Murray* [2007] for the tidal marsh platform evolution couples erosion by tidal current and sediment deposition with vegetation. In a similar way *D'Alpaos et al.* [2006] modeled the cross section of a tidal channel coupling tidal flow, distributed shear stress,

[1]Department of Earth Science and Center for Computational Science, Boston University, Boston, Massachusetts, USA.
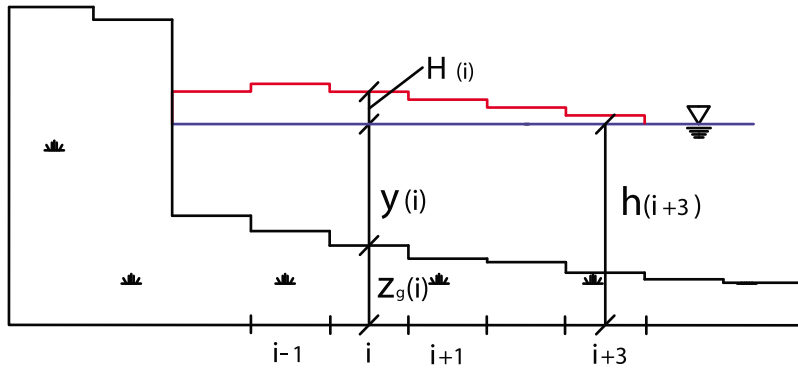
Figure 1. Model geometry. The tidal flat/salt marsh transect is divided into cells of width dx. The cells are numbered from left to right.

and vegetation. In both cases the vegetation was a function of elevation and therefore was linked to the morphological evolution of the system.

[6] In the context of marsh boundary erosion, *van de Koppel et al.* [2005] presented a model that simulates the evolution of the scarp boundary as a function of vegetation biomass and waves. This simple model, based on few phenomenological equations, is extremely effective in capturing the long-term evolution of the system and paved the way to a new generation of high-resolution models, which will include a physically based description of the processes at play. Here we expand this approach by including wave generation and propagation, tidal oscillations, sediment transport, and the feedbacks between vegetation and sediment deposition. The model couples two distinct modules for salt marsh and tidal flat morphodynamics through the exchange of sediments and the erosion/progradation of the marsh boundary.

[7] We utilize an ecogeomorphic model of salt marsh evolution which includes feedbacks between marsh vegetation and sediment transport [see *Fagherazzi and Sun*, 2003; *D'Alpaos et al.*, 2005, 2006]. The model couples a hydrodynamic module to the vegetation framework delineated by *Morris et al.* [2002] and *Mudd et al.* [2004] to quantify the feedbacks between vegetation and sediment fluxes. Specifically, vegetation biomass, belowground production, and sediment trapping by plants are all implemented as a function of marsh elevation and allowed to covary over time with marsh landforms. In the tidal flats we use a previously developed model, which quantifies the influence of tidal currents and wind waves on tidal flat equilibrium [*Fagherazzi et al.*, 2006, 2007; *Defina et al.*, 2007]. The model accounts for sediment deposition and sediment resuspension by wind waves as a function of bottom characteristics, as well as for the erosion of the marsh scarp produced by breaking waves.

2. Coupled Salt Marsh–Tidal Flat Model

[8] The numerical model is implemented on an intertidal transect perpendicular to the marsh boundary which includes both a tidal flat and a marsh platform (Figure 1). The transect is divided into N cells of width Δx, set equal to 0.1 m to have enough spatial resolution. z_g (i) and $y(i)$ are the bottom elevation and the water depth associated with the cell i (Figure 1). An open ocean or tidal basin is assumed on the

right boundary $(i = N)$, from where wind and tides propagate into the domain. An impermeable wall is assumed on the left boundary, corresponding to upland $(i = 1)$.

[9] The physical processes included in the domain are: wind-induced waves, tidal currents, sediment erosion, transport and deposition. The model takes also into account the dynamics of marsh vegetation and its feedbacks with erosion and deposition processes.

2.1. Wind-Induced Waves, Tides, and Related Bottom Shear Stresses

[10] Wave propagation is described by the one-dimensional equation of wave energy conservation at steady state:

$$c_g \frac{dE}{dx} = S \tag{1}$$

where E is the wave energy, $c_g = \frac{\sigma}{2k}(1 + \frac{2ky}{\sinh(2ky)})$ is the wave group celerity, y the water depth, σ the wave frequency, and k the wave number. The source term S is described by the following equation:

$$S = S_w - S_{bf} - S_{wc} - S_{brk} \tag{2}$$

where S_w is the wave growth by wind action on the water surface, and the other terms are the dissipation of wave energy by bottom friction (S_{bf}), whitecapping (S_{wc}) and depth-induced breaking (S_{brk}). The source term can be expressed as a function of wind speed (blowing from right to left), water depth and wave energy; it reads

$$S = \alpha + \beta E - 2C_f \frac{k}{\sinh(2ky)} E - c\sigma \left(\frac{\gamma}{\gamma_{PM}}\right)^m E - \frac{2a}{T} Q_b \left(\frac{H_{max}}{H}\right)^2 E \tag{3}$$

The values of the parameters α and β depend on the wind speed U, C_f is a dissipation coefficient, γ is the integral wave steepness parameter, i.e., $\gamma = E\sigma^4/g^2$, σ is the relative frequency, γ_{PM} is the theoretical value of γ for a Pearson-Moskowitz spectrum, Q_b is the probability that waves with height H will break, T is the wave period, c, m and α are empirical parameters. The numerical values of the parameters utilized to solve equation (3) are reported by *Fagherazzi et al.* [2006] and *Carniello et al.* [2005].

[11] Equation (1) is solved imposing an energy wave value equal to zero at the seaward boundary and propagating the wave energy along x using an upwind scheme in space:

$$E(i - 1, t) = E(i, t) + S(i, t)\Delta x / c_g(i, t) \qquad (4)$$

where i is the element location (see Figure 1). From the linear wave theory the wave height is derived from the wave energy, $H = \sqrt{8E/\rho g}$, where g is the gravitational acceleration and ρ the water density. The bottom shear stress induced by the wave is calculated using the computed wave height [*Fredsoe and Deigaard*, 1992]:

$$\tau_{wave} = \frac{1}{2} f_w \rho \left(\frac{\pi H}{T \sinh(ky)} \right)^2 \qquad (5)$$

where f_w is a friction factor and T is the wave period, assumed constant during propagation. For computational stability the shear stress induced by waves is set equal to zero when the water depth is shallower than 1 cm. Given the small dimension of the domain, the tide is assumed to propagate with infinite speed, therefore we set the water level h equal at every point of the domain and varying only in time following tidal oscillations. The tide is assumed harmonic and semi-diurnal, without spring neap modulation:

$$h(t) = A \sin\left(t \frac{2\pi}{12} \right) \qquad (6)$$

where A is half of the tide range and t is time in hours.

[12] Tidal currents are calculated with a quasi-static model, based on the continuity equation:

$$Q(i + 1, t) = Q(i, t) - \frac{\Delta y}{\Delta t} \Delta x \qquad (7)$$

where y is the water depth, equal to $h - z_g$ (and zero if $h < z_g$), Q is a discharge per unit width, positive if directed rightward, and assumed equal to zero on the landward boundary, i.e., $Q(i = 1, t) = 0$.

[13] Bottom shear stress induced by the tidal current is calculated with an equation for uniform flow:

$$\tau_{curr} = C_f \rho (Q/y)^2 \qquad (8)$$

where ρ is the water density and C_f is a friction coefficient set equal to 0.01 [*Fagherazzi et al.*, 2007]. The total bottom shear stress is calculated as a nonlinear combination of wave shear stress and tidal current shear stress [*Soulsby*, 1997]:

$$\tau = \tau_{wave} + \tau_{curr} \left[1 + 1.2 \left(\frac{\tau_{wave}}{\tau_{curr} + \tau_{wave}} \right)^{3.2} \right] \qquad (9)$$

2.2. Sediment Erosion and Deposition

[14] The evolution of the tidal flat bottom is governed by erosion and sedimentation processes, according to the Exner equation:

$$\rho_b \frac{dz_g}{dt} = D - R \qquad (10)$$

where ρ_b is the sediment density, D is the sedimentation rate and R is the erosion rate. The erosion term is the sum of two terms:

$$R = R_{shear} + R_{break} \qquad (11)$$

The first term is given by bottom shear stresses induced by waves and currents, whereas the second term captures the effect of turbulence generated by wave breaking. The simplest and widely used formulation for bottom erosion is

$$R_{shear} = \begin{cases} 0 & \tau < \tau_{cr} \\ \alpha(\tau - \tau_{cr}) & \tau > \tau_{cr} \end{cases} \qquad (12)$$

where α is the erosion rate and τ_{cr} is the critical shear stress.

[15] The second term, R_{break}, takes into account the localized erosion induced by the breaking of the waves.

[16] We propose a formulation with the structure of the classical erosion equation, using wave power as main variable:

$$R_{break} = \begin{cases} 0 & P < P_{cr} \\ \beta(P - P_{cr})/d & P > P_{cr} \end{cases} \qquad (13)$$

where β is a constant parameter, P is the wave power per surface unit dissipated by breaking, P_{cr} is a threshold value for erosion, and d is the length over witch the erosion by wave breaking takes place, here equal to the cell length.

[17] Contrary to bottom erosion, which is a continuous process for a given wave forcing, scarp erosion is a discontinuous process, with removal of surface particles superimposed to scarp failure and mass wasting. For example, *Allen* [1990] showed that scarp erosion chiefly occurs through toppling and rotational slip. Moreover, vegetation has a strong role in scarp resistance and erosion mechanisms, and clearly its influence cannot be addressed with a standard wave breaking formulation on a gentle slope.

[18] To our knowledge, there are no detailed models that describe the physics of the erosion of a cohesive marsh scarp by wave attack. The equation that relates sediment erosion to excess shear stress (equation (12)) cannot be used on a vertical scarp since the shear tensor is different than the one acting on a horizontal bottom. In fact, while at the bottom only the tangential shear stress is present (excluding the constant hydrostatic pressure), on the vertical scarp both tangential and normal stresses promote erosion.

[19] Given the complexity of the process of scarp erosion, a heuristic approach based on only one parameter seems a better choice for a long-term model of marsh evolution. This parsimonious strategy is commonly adopted in geomorphic models of river meanders, in which the erosion of vegetated river banks is simply set proportional to the flow velocity at the river outer bank [*Pizzuto and Meckelnburg*, 1989; *Seminara*, 2006]. Similarly, *Schwimmer* [2001] correlates the long-term erosion rate of marsh scarps to the averaged wave power.

[20] We thus propose to use the same equation for bottom erosion by wave breaking (equation (13)), in which the term P is set equal to the rate of power dissipation by wave impact
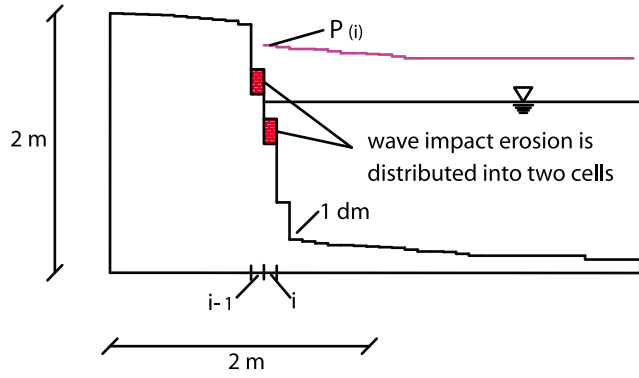
Figure 2. Schematic of the wave impact erosion on a vertical scarp.

at the marsh scarp. When the wave encounters a vertical wall, the water depth becomes suddenly equal to zero, and the breaking is localized in a small area in which the wave loses all its energy. In this case the breaking energy should be spread along a vertical surface, which cannot be represented in a 1-D model. To reproduce this process, we distribute the breaking energy into the two cells defining the scarp, namely the one above and the one below the point where the water encounters the bottom (see Figure 2). Operatively, we set the value of P equal to Ec_g to both cells in equation (13), where the wave energy and the group celerity are calculated in the last cell with water depth greater than zero, and d is equal to two cell lengths.

[21] With this formulation the erosion by wave impact does not induce a horizontal migration of the scarp, but rather a vertical erosion of a cell column. However, by splitting the erosion into two cells and using a fine spatial resolution (0.1 m), we obtain a macroscopic result that well agrees with the characteristics of scarp erosion by lateral migration (Figure 2). It should be stressed that scarp erosion is a complex phenomenon, which takes place both by gradual regression of the scarp, and by macroscopic failures. Our formulation could be seen as the average result of the two processes.

[22] We use a value for P_{cr} that ranges from 3 W to 15 W, depending on vegetation. These values correspond to a range of wave height of 7–15 cm (assuming a wave group celerity of 0.5 m/s, which is a common value in front of marsh boundaries). This range of wave height matches the range of threshold values individuated by *Trenhaile* [2009] in his model for steeply sloping bluff retreat by broken wave impact. The value of β is calibrated empirically to have a regression rate of the order of m/yr. We recognize that further study have to be performed to determine the role of geotechnical parameters on scarp erosion.

[23] The sedimentation rate is estimated with the formula of *Einstein and Krone* [1962]:

$$D = \begin{cases} 0 & \tau > \tau_d \\ w_s r C \left(1 - \dfrac{\tau}{\tau_d}\right) & \tau < \tau_d \end{cases} \quad (14)$$

where w_s is the settling velocity, r is an empiric coefficient set equal to 2 [*Parker et al.*, 1987], τ_d is the shear stress below which the sediment deposits.

[24] The average sediment concentration in the water column is calculated by imposing the conservation of mass:

$$\frac{\partial(yC)}{\partial t} + \frac{\partial(QC)}{\partial x} + \varsigma \frac{\partial^2(yC)}{\partial x^2} = R - D \quad (15)$$

where ς is the diffusion coefficient, and C is the sediment concentration.

[25] The advection-diffusion equation is discretized in space with a central difference scheme for the diffusion term and with an upwind method for the advection term. For stability purposes the system is solved implicitly in time. The resulting nonsymmetric linear system is solved with a preconditioned biconjugate gradient method. In addition, for computational efficiency, the cells used for the advection-diffusion equation is larger (2 m) than the bottom cells (0.1 m).

2.3. Vegetation Processes

[26] The presence of vegetation greatly modifies erosion and deposition processes on the marsh platform. The vegetation canopy decreases wave height and current velocity; roots increase the sediment resistance to erosion, vegetation biomass favors mineral sediment trapping and promotes belowground organic production.

[27] *Mudd et al.* [2004] modeled all these processes as a function of aboveground biomass B. Using the data of *Morris et al.* [2002], *Mudd et al.* [2004] described the biomass as a function of the elevation relative to the tide, D, defined as the difference between the HAT (highest astronomical tide) and the ground elevation. This value is biunivocal linked to the time fraction during which the vegetation is submerged [*Mudd et al.*, 2004]. The biomass is zero when is submerged for too long (D_{max}), and when it is not submerged long enough (D_{min}). Following *Morris* [2006] we assume that vegetation biomass varies parabolically within D_{min} and D_{max}:

$$B_{ps} = \begin{cases} 0 & D < D_{min} \\ B_{max}(aD + bD^2 + c) & D_{min} < D < D_{max} \\ 0 & D > D_{max} \end{cases} \quad (16)$$

The parameters a, b, and c are chosen in order to have B equal to zero at $D = D_{max}$ and $D = D_{min}$, and equal to B_{max} at the parabola maximum.

[28] Vegetation biomass varies through the seasons, peaking in the summer months, as shown by *Morris and Haskin* [1990]. *Mudd et al.* [2004] proposed the following formulation:

$$B = \frac{B_{ps}(1 - \omega)}{2} \left[\sin\left(\frac{2\pi m}{12} - \frac{\pi}{2}\right) + 1 \right] + \omega B_{ps} \quad (17)$$

where B is the biomass, m is the month, with $m = 1$ corresponding to January, and ω is a dimensionless factor.

[29] Vegetation increases the sediment's resistance to erosion by stabilizing the substrate with a root mat. In our model we linearly correlate the increase of erosion threshold with the aboveground biomass:

$$\tau_{cr} = \tau_{cr}\left(1 + K_{veg}B/B_{max}\right) \quad (18)$$

where K_{veg} is a nondimensional parameter.

Wave & tide computation biomass evaluation	H (i), Q (i), B (i)
Erosion rate evaluation	E (i)
Bottom erosion and sediment update	Zg(i), C (i)
Sediment advection-diffusion	C (i)
Deposition rate evaluation	D (i)
Sediment deposition and bottom update	Zg(i), C (i)

t=t+1
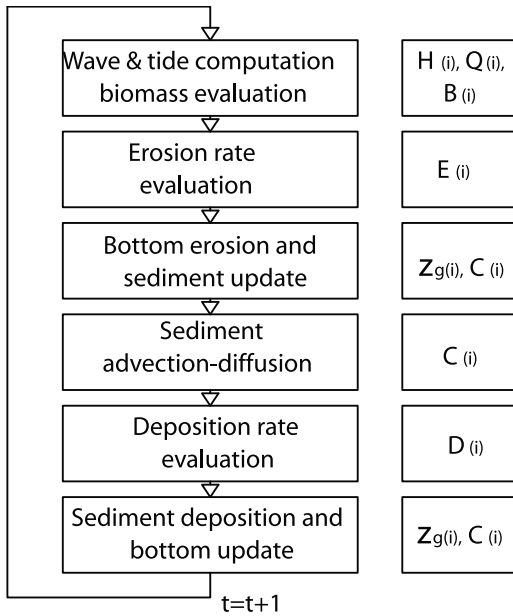
Figure 3. Model flowchart.

[30] Vegetation plays also a role in the erodibility of the scarp. Only the top layer of marsh cliffs is resistant, because a dense root mat of marsh grasses binds the sediments together. We assume that the root mat is directly related to the above ground biomass, and that once the biomass is removed, also the roots (or their stabilizing effect) disappear. Moreover, we assume that vegetation linearly increases the critical energy P_{cr} for wave erosion as a function of biomass (see equation (13)):

$$P_{cr} = P_{cr}\left(1 + K_{veg}B/B_{\max}\right) \qquad (19)$$

Vegetation influences sedimentation processes as well, by increasing the sediment trapping efficiency, and the below-ground organogenic production.

[31] The vegetation effect on the sedimentation rate is expressed by

$$D = D_s + D_t \qquad (20)$$

Where D_s is the sedimentation rate due only to settling. The rate of sediment trapped by vegetation D_t is expressed by the following equation:

$$D_t = Cu\eta d_s n_s h_s \qquad (21)$$

where u is a typical value of the flow speed through vegetation, η is the rate at which transported sediment particles are captured by plant stems, d_s is the stem diameter, n_s is the stem density per unit area, and h_s is the average height of the stems. Accordingly to the formula proposed by *Palmer et al.* [2004], the capture efficiency η reads

$$\eta = 0.224\left(\frac{ud_s}{\nu}\right)^{0.718}\left(\frac{d_p}{d_s}\right)^{2.08} \qquad (22)$$

where d_p is particle diameter, and ν is the water kinematic viscosity.

[32] The values of stem density per unit area, n_s, stem diameter, d_s, and average stem height, h_s, are expressed as a function of the above ground biomass B [*Mudd et al.*, 2004]:

$$\begin{aligned} n_s &= 250B^{0.3032} \\ h_s &= 0.0609B^{0.1876} \\ d_s &= 0.0006B^{0.3} \end{aligned} \qquad (23)$$

Above ground biomass also promotes organogenic sediment production. The linear relationship between organogenic sedimentation and biomass presented by *Randerson* [1979] is chosen in this model:

$$z_g = z_g + k_b B/B_{\max}\Delta t \qquad (24)$$

where k_b is the maximum sedimentation rate.

[33] The vegetation canopy on the marsh surface attenuates wind waves. *Möller* [2006] studied wave attenuation induced by marsh vegetation in a UK salt marsh, finding a correlation between wave attenuation and the ratio wave height/water depth. Wave attenuation over a 10 m transect varied from 0.008% to 33%, depending on water depth and vegetation. For simplicity, we assume that the relative attenuation per unit of length along the direction of propagation is proportional to the vegetation biomass, with a maximum value of 3% per meter when the maximum biomass is reached. The relationship is

$$H_{reduction}(\%) = 3\frac{B}{B_{\max}}L_{Att} \qquad (25)$$

where L_{Att} is the length along which the wave propagates, expressed in meter.

2.4. Computational Scheme

[34] At every time step both the bottom elevation z_g and the water depth y are held constant in every cell, while wave height, tidal current, and total shear stress are computed with equations (3), (7), and (9), respectively. The erosion rate is calculated with equation (11) and the bottom elevation and suspended sediment are updated maintaining the mass balance:

$$z_g^{t+1/2} = z_g^t - R\Delta t/\rho_b \quad C^{t+1/2} = C^t + R\Delta t/y^t \qquad (26)$$

The advection-diffusion equation (equation (15)) is applied for a time step, then the sedimentation rate is calculated and the bottom elevation and the suspended sediment are updated:

$$z_g^{t+1} = z_g^{t+1/2} + D\Delta t/\rho_b \quad C^{t+1} = C^{t+1/2} - D\Delta t/y^t \qquad (27)$$

Finally the biomass is recalculated as a function of elevation. The computational flowchart is presented in Figure 3.

[35] In order to have sufficient resolution during a full tidal cycle, a time step $dt = 30$ min is chosen. To reduce the simulation time we use a higher model resolution during strong wind conditions and a lower model resolution during weak wind conditions. The simulation is divided into storms,
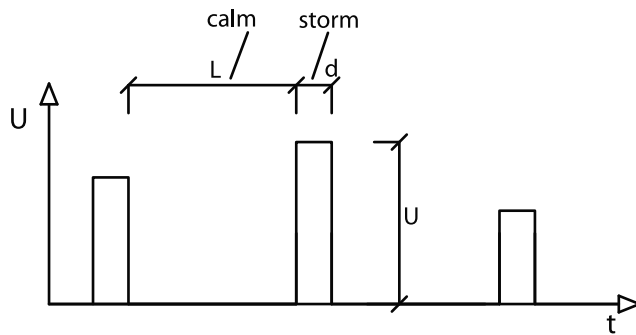
Figure 4. Numerical representation of wind events. Periods with constant wind velocity U are spaced by periods of fair weather ($U = 0$).

during which the wind speed U is greater than a certain threshold, and fair-weather conditions, during which the wind speed is zero. The simulation is a sequence of storms and fair-weather periods, with duration d and L, respectively (Figure 4). During a storm the model runs with resolution Δt. During fair weather the system evolution is computed using only two tidal cycles, both calculated with resolution Δt and wind speed set to zero. In the first cycle the model is run normally, in the second cycle the model is run using a multiplying factor for sedimentation. This allows simulating sediment deposition with less computational time.

[36] The wave height at the seaward boundary cell is not imposed, but it is calculated propagating an initial wave of 1 cm height over a horizontal flat with water depth equal to the water depth at the seaward boundary cell. This allows the utilization of an arbitrary wind fetch without increasing too much the computational effort. During the simulation the fetch length has been kept equal to 3 km. The model parameters are summarized in Table 1.

3. Results

[37] Three sets of simulations are performed, with different scenarios of sediment availability. All simulations are run with and without vegetation, maintaining constant all the other parameters. The wind speed is assumed to be a random variable uniformly distributed between 0 and 20 m/s, the duration of the storm times, d, are 12 h, the duration of the calm times, L, are 10 days, the wave period, T, is 2 s, the tidal amplitude, A, is 2 m.

[38] In the first set of simulations the total mass of sediment is maintained constant and conservative boundary conditions for the advection-diffusion equation are used. Specifically, the maximum possible deposition in each cell is limited to the volume of suspended sediment in the water column above that cell. The model starts with an initial condition of a tidal flat with a gentle slope (3:1000) below MSL and no sediment in suspension. The simulation is run until a steady configuration is reached after 200 years.

[39] Figure 5 shows the steady state profiles with and without vegetation. In both cases the tidal flat evolves into a concave-up profile, with a marsh (or an unvegetated terrace in the simulation without vegetation) that forms on the upper part of the profile, at the landward side. The elevation of the salt marsh is close to HAT (highest astronomical tide with a

gentle slope (2:1000). The transition between tidal flat and salt marsh takes place with a variation of the profile slope. In the simulation without vegetation the transition is gentle, with a gradual change from a convex up to a concave up profile. When the vegetation is present the slope increases from 2:1000 to 2:1 in few meters, creating a scarp.

[40] In order to evaluate the model sensitivity to the spatial discretization, we perform the same simulation (scarp evolution starting from a constant slope with conservation of sediments), with dx = 0.1 m and dx = 0.05 m. The results of the two simulations are identical in time. Moreover, only for a very large cell sizes some differences are visible.

[41] In the second set of simulations we reproduce the infilling of a tidal basin (Figure 6). The initial condition is a tidal flat with a level 2 m lower than LAT (lowest astronomical tide), and the sediment concentration on the seaward boundary cell is set equal to 0.5 g/l. The net inflow of sediments leads to marsh accretion (Figures 6a and 6b). In both cases (with and without vegetation) sediments start to accumulate at the landward side, maintaining a concave-up shape, with a gradual steepening of the deposit's slope. When the accreting area is close to HAT, the sediments form a terrace and a change in concavity takes place. After this point the whole profile prograde with a rigid translation, without variations in shape. When the vegetation is absent (Figure 6a) the progradation ends when the system finds an equilibrium with the sediment input (after 300 years of simulation the profile does not change anymore). The equilibrium shape is similar to the one achieved imposing the conservation of sediment volume. When the vegetation is present (Figure 6b) the profile does not reach equilibrium, and the system tends to fill the entire tidal basin. The slope between salt marsh and tidal flat is steeper (1:15) than in the case without vegetation (1:50), but the vertical scarp is still absent.

[42] In the third set of experiments we simulate the erosion of salt marshes in a tidal basin (Figure 7). In this case the initial configuration is set equal to the configuration reached after 150 years of basin infilling with vegetation (see Figure 6b). In order to remove sediment from the basin, the sediment concentration at the seaward boundary cell is set equal to a low value (0.1 g/l), so that a net sediment flux exits the domain. In both simulations, with and without vegetation, erosion lowers the tidal flat over time by about 0.5 m. When vegetation is absent erosion takes place on the top of the scarp, creating a gentle profile (Figure 7a). During the last

Table 1. Model Parameters

Parameter	Value	Author
P_{cr}	3 W	Tuned for the model by the authors
β	1.4 10^{-5} kg/J/m	Tuned for the model by the authors
k_b	0.009 m/year	*Blum and Christian* [2004]
B_{max}	2000 g/m^2	*Mudd et al.* [2004]
D_{min}	0.1	*Morris* [2006]
D_{max}	0.9	*Morris* [2006]
ω	0.1	*Mudd et al.* [2004]
ς	0.5 m^2/s	*Chapra* [1996]
K_{veg}	5	*Le Hir et al.* [2007]
ν	10^{-6} m^2/s	
ρ	1023 kg/m^3	
ρ_b	1800 kg/m^3	*Fagherazzi et al.* [2007]
τ_d	0.1 Pa	*Parchure and Metha* [1985]
τ_{cr}	0.7 Pa	*Amos et al.* [2004]
α	4.12 10^{-4} kg/(m^2 s Pa)	*Cappucci et al.* [2004]
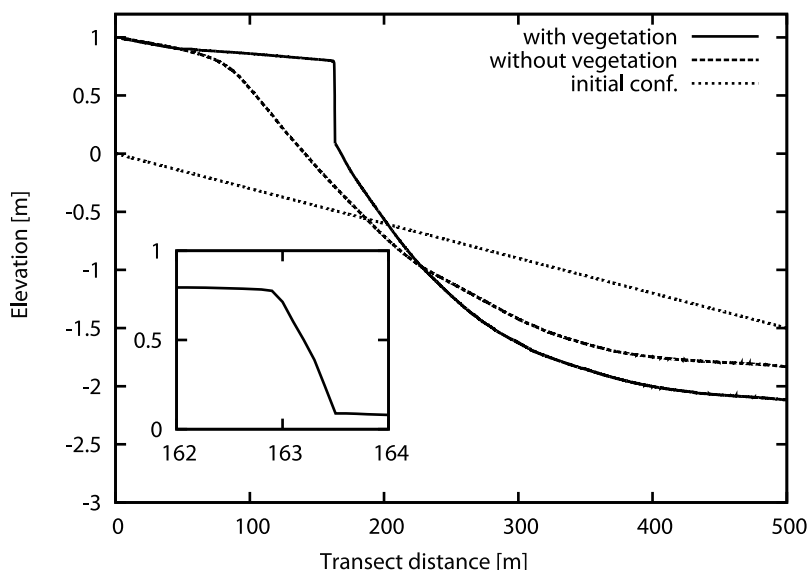
Figure 5. Steady intertidal profile after 200 years of simulation. The initial topography was a gently sloping tidal flat below mean sea level. The total amount of sediments is conserved during the simulation. The inset shows a detail of the marsh boundary.

stages of the erosion process, the slope of the platform becomes steeper and eventually a vertical scarp forms. At this point the regression of the platform is given by a translation of the scarp. The erosion of the scarp continues until all sediments are removed from the basin. When vegetation is present, the upper part of the marsh is not eroded (Figure 7b). The erosion concentrates at the foot of the marsh, and a vertical scarp forms after a short time. Once the scarp is created, the erosion of the marsh is given by a rigid translation of the boundary. The height of the scarp remains constant in time, at 1 m.

[43] Figure 8 shows the elevation distribution in the basin with vegetation, during infilling (Figure 8a) and during erosion (Figure 8b). In both cases the distribution is bimodal, with one peak corresponding to the tidal flat elevation and one corresponding to the salt marsh elevation [see also *Fagherazzi et al.*, 2006].

[44] In the last set of simulations the effect of Relative Sea Level Rise (RSLR) is taken into account. Figure 9 shows the simulation of the erosion of the marshes with a constant RSLR of 2 mm/yr. As in the simulation with no RSLR, when the vegetation is present a vertical scarp forms, but in this case the regression is faster (about 1.5 times), and the height of the scarp increases in time, reaching a maximum of about 1.5 m (Figure 9b). When the vegetation is absent, no vertical scarp forms, not even at the last stages of the erosion process (Figure 9a).

[45] In Figure 10 we simulate the coupled salt marsh–tidal flat evolution under different rates of sea level rise. Only the simulation with vegetation is reported. When the RSLR is low, 2 mm/yr, the marsh is prograding (Figure 10a). The slope between the marsh and the tidal flat is steeper (1:5) than in the case without RSLR, but without a distinct vertical scarp. With a RSLR of 10 mm/yr the marsh is close to equilibrium (Figure 10b). The marsh initially prograding and then regrades with a very slow rate (about 0.03 m/yr). With a RSLR of 20 mm/yr the scarp instead regrades (Figure 10c), with a fast rate (about 0.5 m/yr). With a RSLR of 30 mm/yr

the scarp initially regrades and then eventually drowns (Figure 10d).

[46] Figure 11 shows the values of marsh boundary horizontal displacement rate (i.e., progradation or erosion) as a function of RSLR and sediment concentration at the seaward boundary. For simplicity we indicate erosion as negative progradation. For every combination of RSLR and sediment concentration platform progradation is higher when vegetation is present. Moreover, in the vegetated case, the relation between progradation (p), RSLR and boundary sediment concentration (C) is approximately linear (Figure 11a). The sensitivity of the horizontal displacement rate on RSLR and sediment concentration is different whereas the marsh is prograding ($p > 0$) or eroding ($p < 0$). The following set of equations best fits the data:

$$p = -7.8 \times RSLR + 275 \times C - 75.5 \quad p > 0$$
$$p = -3.5 \times RSLR + 110 \times C - 26 \quad p < 0 \qquad (28)$$

where p is expressed in cm/yr, RSLR is expressed in mm/yr, C is expressed in g/l. Under progradation conditions the sensitivity of the horizontal displacement to RSLR and sediment concentration is more than double that under erosion condition (see the coefficients multiplying RSLR in equation (28)).

[47] When vegetation is absent, the sensitivity of the marsh horizontal displacement rate with RSLR is higher under progradation than under erosion (Figure 11b). Moreover, the relationship between progradation rate and sediment concentration remains approximately linear.

4. Discussion and Conclusions

[48] The present model is a development of the model proposed by *van de Koppel et al.* [2005]. Our model does not produce the self-organized cycle of scarp erosion episodes which are present in the *van de Koppel et al.* [2005] model. We suggest three possible reasons for this discrepancy.
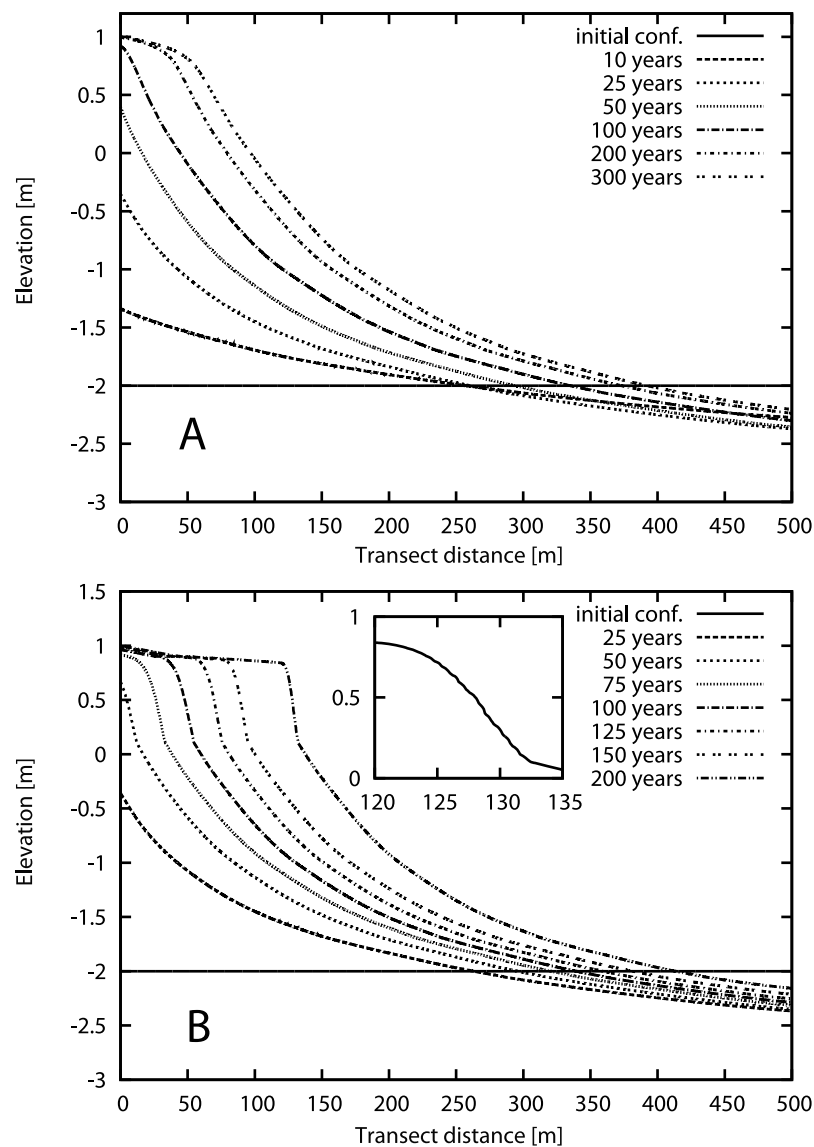
Figure 6. Basin infilling. The evolution of the profile starts from a horizontal tidal flat, with a constant sediment concentration (0.5 g/l) at the seaward boundary. (a) Without vegetation and (b) with vegetation. The marsh is defined as the zone where the marsh vegetation can grow, and tidal flat is defined as the zone where the marsh vegetation cannot grow.

[49] First, in the model of *van de Koppel et al.* [2005] the system is subject to a constant external forcing; that is, wave erosion is a function of a parameter that is constant over the simulation. In our model the system is instead subject to alternate events of fair weather and wind. This more realistic situation allows the system to escape from conditions of positive erosive feedback, which cause the erosion cascade described by *van de Koppel et al.* [2005]. For example, during a long period without wind, the cliff can find a more stable configuration, depositing sediment at the scarp toe, thus reducing incoming waves and therefore stopping erosion.

[50] Second, in the model of *van de Koppel et al.* [2005] wave erosion is a function of bottom slope and biomass, which are defined locally and do not depend on the entire landscape morpholology. On the contrary, in our model wave erosion is also a function of tidal flat elevation, which affects

wave propagation and therefore the amount of energy reaching the scarp. This global coupling makes the model less dependent on local unstable conditions.

[51] Third, in the model *van de Koppel et al.* [2005] a vertical scarp is inherently unstable, since erosion is proportional to bottom slope. This model component triggers the erosion cascade, since the steeper is the scarp the more unstable it becomes. In our model a vertical scarp is instead stable, thus mimicking the natural conditions of many tidal marsh boundaries.

[52] The model assumes a 1-D geometry. This simplification cannot address lateral variations in salt marsh, tidal flat, and scarp morphology. Regarding the salt marsh, the 1-D geometry does not address the presence of tidal creeks, which promote marsh drainage and therefore limit the erosion by sheet flow. However, the percentage of marsh area covered by creeks is generally low, and large stretches of marsh scarp
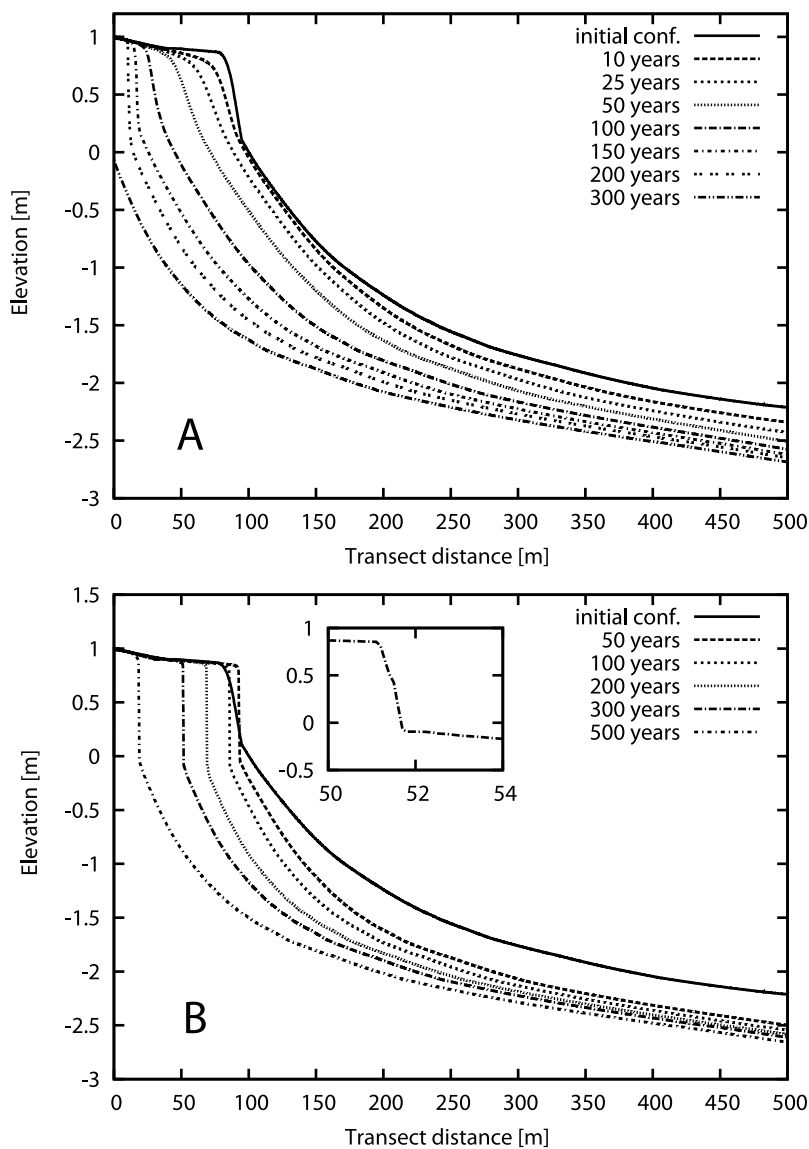
Figure 7. Salt marsh deterioration. The evolution of the profile starts from a fully developed salt marsh, imposing a sediment concentration equal to 0.1 g/l at the seaward boundary: (a) without vegetation and (b) with vegetation.

are not affected by them. Therefore we can assume that our transect is far enough from tidal creeks without loss of generality. At the boundary between the marsh and the tidal flat, the 1-D geometry prevents the reproduction of complex erosional features, like transversal incisions, gullies, and toe undercutting. These features might induce different rates of boundary erosion, and will be addressed in future research.

[53] The 1-D assumption also prevents simulating the formation of drainage channels in tidal flats. Tidal channels concentrate tidal currents, reducing the flow in the remaining tidal flat. The channels promote the local transport of sediments, leading to a global increase in sediment mobility. This effect can be simulated increasing the suspended sediment diffusion in our model (the parameter ζ in equation (15)). However, all these processes do not directly affect the local scarp evolution, which is the key point of this study. Future research will address the role of channels on the coupled evolution of tidal flats and salt marshes.

[54] The spatial discretization introduces an additional source of error since the verticality of the scarp is limited by the finite cell dimension (0.1 m). Therefore the model cannot exactly represent a vertical scarp or a protruding one. However, our simplified discretization is computationally very efficient, and it is sufficient to simulate the scarp evolution in time. We assume that erosion by wave impact only acts in the two cells defining the scarp, and a sensitivity analysis has shown that different cell sizes lead to identical results.

[55] Simulations show that in an intertidal area in which the total amount of sediment is conserved the cross-shore profile evolves until forming a platform above mean sea level and a tidal flat below mean sea level. The profile evolution is faster when the system is far from this equilibrium configuration, such as when the initial bathymetry is horizontal or with constant slope. In the initial stages of the evolution there are zones along the tidal flat profile where erosion, both by
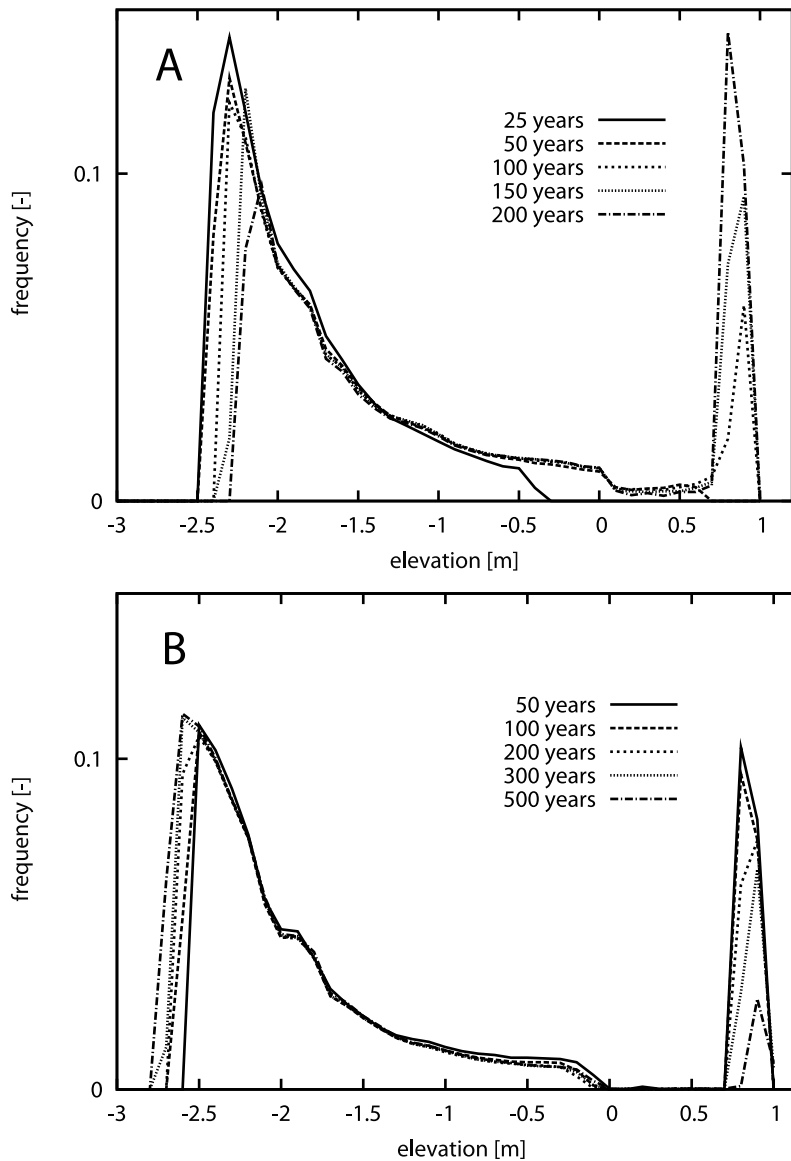
Figure 8. Frequency distribution of basin elevation during the simulation (vegetated case). (a) Basin infilling. (b) Basin erosion.

shear stress and wave breaking, is concentrated. On the contrary, close to the final equilibrium configuration, erosion rates are almost negligible along the tidal flat. In fact the equilibrium profile of the tidal flat varies gently in space thus preventing wave breaking, but favoring the dissipation of wave energy by bottom friction. Moreover, when the equilibrium configuration is reached, the tidal flat bottom is below the critical shear stress for erosion for most of the time. The concave-up equilibrium profile of the tidal flat resulting from our simulations is in agreement with the results of tidal flat models and field observations [*Pritchard et al.*, 2002; *Waeles et al.*, 2004].

[56] When the intertidal area is encroached by vegetation, and therefore becomes more resistant to wave erosion, a steeper profile develops, with more sediments subtracted from the tidal flat and deposited on the marsh. Is it interesting to note that the tidal flat equilibrium profile is similar with and without vegetation, but just 20 cm lower when vegetation

is present. This indicates that the equilibrium profile stems from the sediment redistribution between the marsh platform and tidal flat, with depositional processes on the marsh platform affecting the neighboring tidal flats.

[57] With a high sediment supply the tidal flats emerge from the water giving rise to a platform. Once the platform is formed, the boundary between the platform and tidal flat prograades, filling the intertidal area. The boundary is steep when vegetation is present and gentle when vegetation is absent. Moreover, vegetation increases the rate of progradation by capturing and stabilizing sediments on the marsh surface. Platform progradation does not develop a clear vertical scarp, even when vegetation is present. On the contrary, a vertical scarp forms when the marsh is under erosion. Scarp formation is a consequence of the lowering of the tidal flat, induced both by low sediment availability or RSLR, which entails that higher waves are reaching the marsh boundary. Vegetation is not critical for scarp develop-
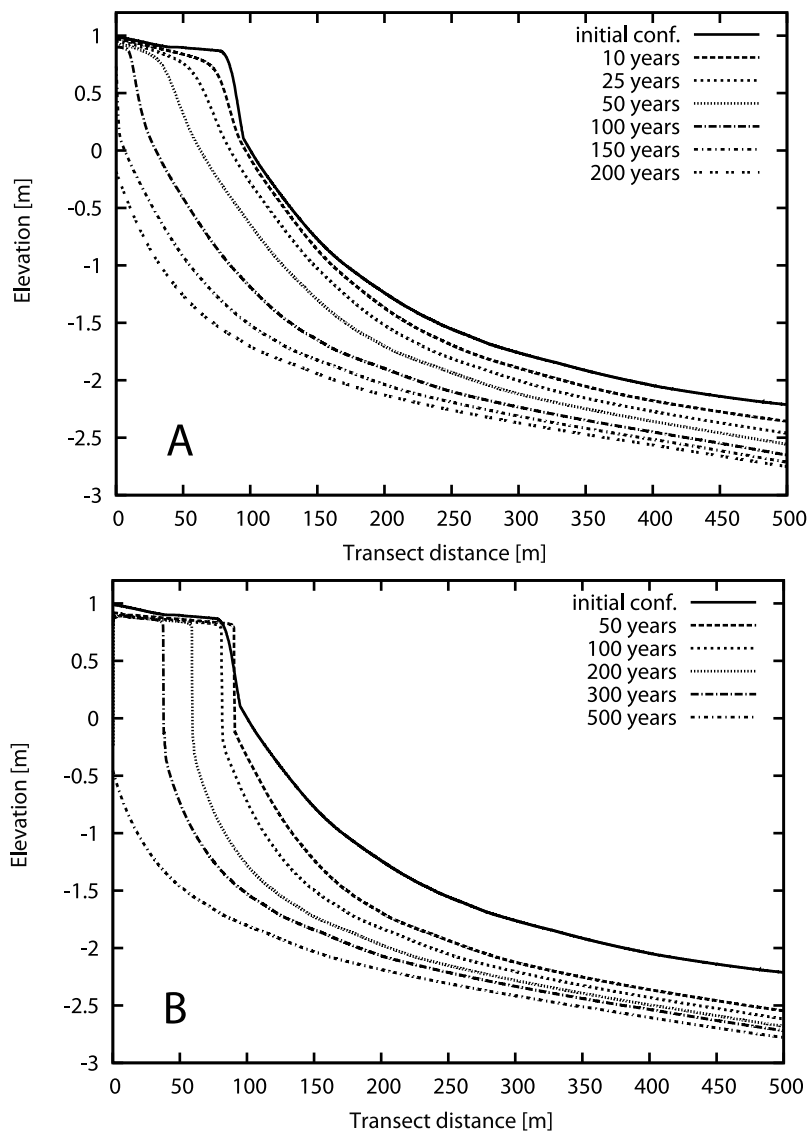
Figure 9. Basin erosion with a RSLR rate of 2 mm/yr. (a) Without vegetation. (b) With vegetation.

ment, since our simulations show that a scarp can form when an unvegetated platform is high in the tidal range (Figure 7a). However, scarp formation is faster when vegetation is present.

[58] The scarp is the location at which most of the wave energy dissipates by breaking. In order to concentrate wave breaking at one location and develop a vertical scarp, two conditions must take place: (1) the tidal flat in front of the scarp has to be flat and enough deep to not significantly dissipate the wave energy before the breaking at the vertical scarp and (2) the scarp must be high enough to concentrate the breaking of the waves for a large range of tidal elevations; that is, also during high tide the wave has to break at the scarp without propagating on the marsh platform.

[59] The top of the marsh scarp is usually subject to high erosion, which in time would replace the scarp with a gentler slope. However, when the marsh is so high that wind waves cannot reach its surface with enough energy, the top of the slope becomes sheltered from erosion, so that wave energy concentrates at the bottom promoting downcutting and the development of a vertical scarp. Vegetation decreases sedi-

ment erodibility and thus protects the high part of the marsh from wave erosion. In addition, vegetation promotes sediment trapping, and therefore accretion. These two mechanisms concentrate erosion in the unvegetated area in front of the marsh, leading to the formation of a vertical scarp.

[60] During the evolution of the intertidal profile, both under marsh progradation and erosion, the distribution of elevations is bimodal, with a distinct marsh and tidal flat separated by a boundary. This underlines that only these two states are stable, and that the highest instability are found in the transition between the two.

[61] RSLR promotes marsh erosion, thus increases the regression rate of the scarp. RSLR submerges the marsh surface, thus promoting erosion not only by wave impact but also by bottom shear stresses, which constantly smooth the marsh edge. Our simulations show that even a small value of RSLR (2 mm/yr) prevents the formation of the scarp when vegetation is absent.

[62] For any given sediment supply, different rates of RSLR entail different qualitative trajectories of basin evolution. A low rate of sea level rise reduces the depth of the tidal
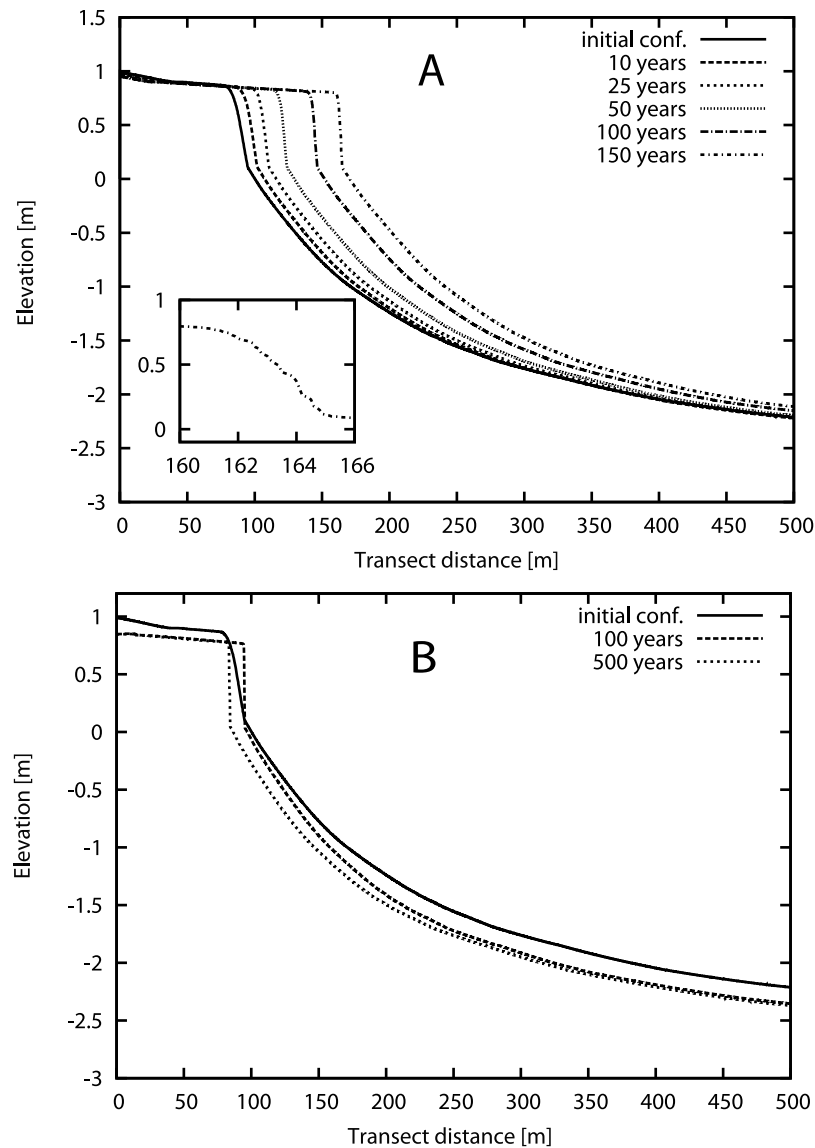
Figure 10. Basin evolution with different RSLR rates and vegetation. The sediment concentration at the seaward boundary is equal to 0.5 g/l. (a) RSLR = 2 mm/yr. (b) RSLR = 10 mm/yr. (c) RSLR = 20 mm/yr. (d) RSLR = 30 mm/yr.

flat increasing wave dissipation. Sediment deposition is thus favored and the marsh boundary prograde. A high rate of sea level rise leads to a deeper tidal flat and therefore higher waves that erode the marsh boundary, leading to boundary retreat. As long as the maximum deposition rate on the marsh is higher than RSLR, the marsh remains emergent. The marsh converges to an equilibrium elevation near the optimum value for vegetation growth (see equation (16)), which is lower than the elevation it reaches without RSLR. This equilibrium is stable because a decrease in salt marsh elevation will increase vegetation biomass and therefore increase erosion resistance and sediment trapping [*Morris*, 2006]. However, the lowering of the tidal flat increases the height of the waves reaching the marsh edge, which results in an increase of marsh regression by wave impact, thus accelerating erosion.

[63] When the rate of RSLR is higher than the maximum deposition rate, there are no possible stable elevations for the marsh platform. In fact when the elevation drops below the optimum value for vegetation growth, the marsh becomes unstable because a reduction in vegetation cover increases erodibility. At this point both wave impact and wave-induced bottom shear stresses will erode the marsh, which eventually drowns, morphing into a tidal flat.

[64] The model results are in accordance with the conceptual model proposed by *Schwimmer and Pizzuto* [2000] based on field observations. The accretion of the marsh, during a period of high sediment supply and low rate of RSLR, occurs by a successive deposition of sediment wedges in front of the marsh boundary. The accreting gentle profile dissipates wave energy, reducing breaking at the salt marsh boundary. Sedimentation on the marsh continues, until HAT is reached. The regression of the marsh is associated with a steepening of the profile, which eventually leads to scarp formation. The results of our model show that both an increase in the rate of RSLR or a decrease in sediment supply
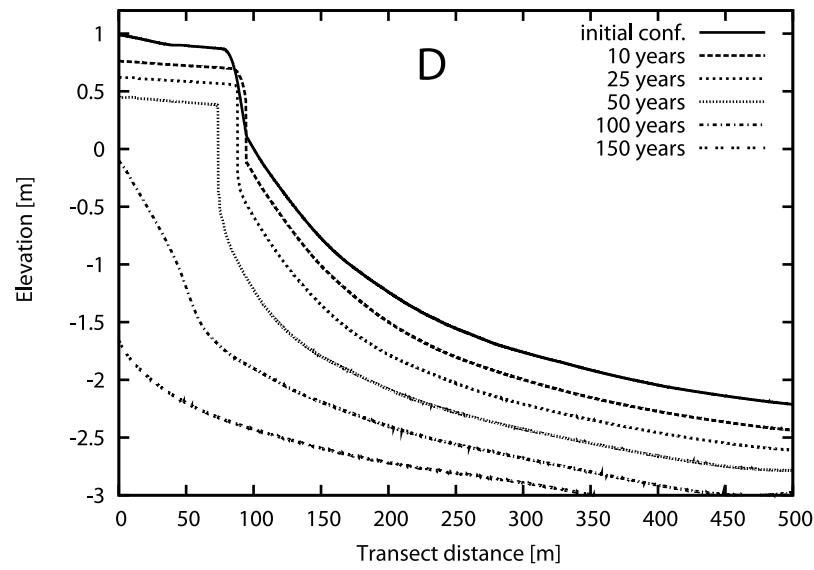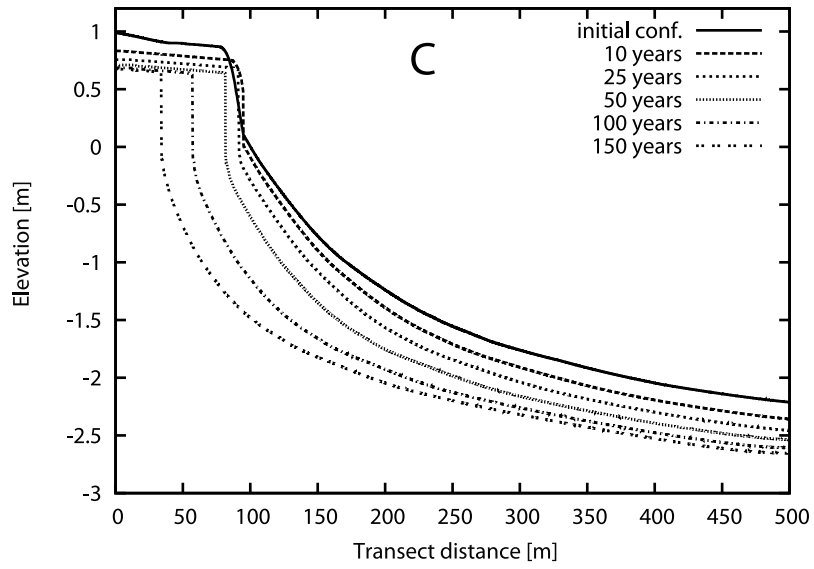
Figure 10. (continued)
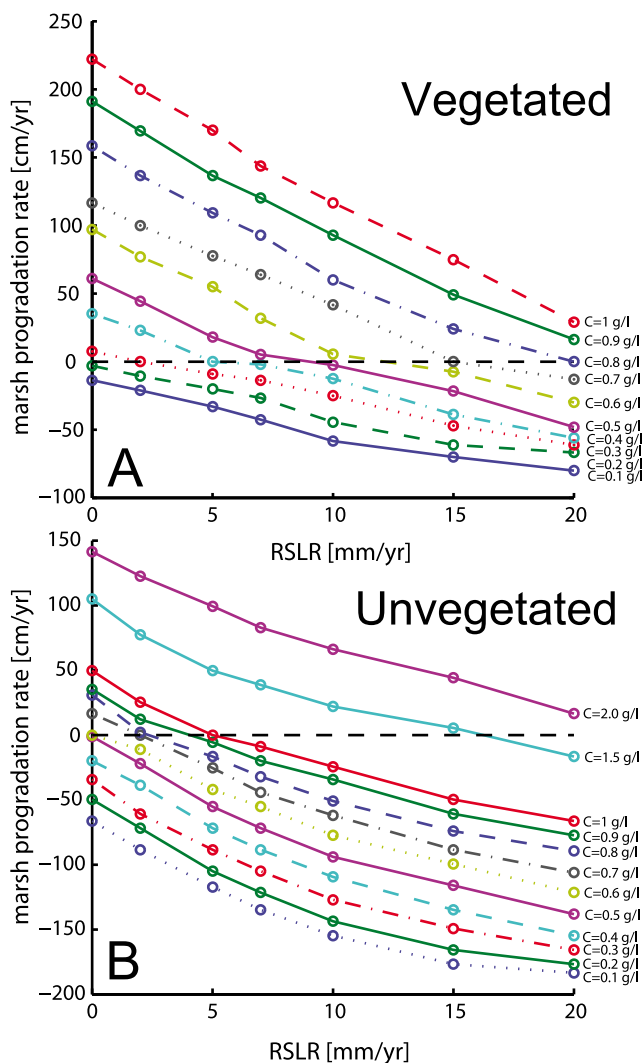
Figure 11. Progradation and erosion rates of the marsh boundary as function of RSLR and sediment concentration. Positive values indicate progradation, and negative values indicate erosion. (a) With vegetation. (b) Without vegetation.

could change the marsh evolutive trajectory from progradation to regression, as indicated by the stratigraphic data of *Schwimmer and Pizzuto* [2000].

[65] Our results are also in agreement with the conceptual model proposed by *Defina et al.* [2007]. During the infilling of the basin the marsh vertically accretes until it reaches a critical elevation; after which the marsh progrades horizontally. Similarly, during basin erosion, the marsh is initially eroded through the horizontal migration of the scarp, until eventually the entire marsh drowns.

[66] Figure 11 summarizes the model results. When vegetation is present marsh progradation dramatically increases at high sediment concentrations and low RSLR. On the contrary, marsh erosion is less sensitive to RSLR and sediment concentration. We explain this phenomenon by considering the different morphologies that the marsh boundary assumes and the different physical processes that take place at the interface. Under progradation the boundary has a gentle slope, more surface is exposed to waves, and therefore an

increase in RSLR will affect a greater surface, leading to a large change in erosive and depositional processes. Instead under regression the marsh boundary becomes a vertical scarp, where all erosion is concentrated. An increase in SLR will affect only a confined zone, reducing the global effect on the intertidal profile. Moreover, progradation is produced by deposition of large volumes of sediments, which can occur in a short time frame (a few tidal cycles are enough to deposit all sediments in suspension). Erosion is instead much slower, since wave attack can erode only a few centimeters of scarp in each storm. Whereas the deposition time scale is fast, the erosion time scale is dictated by the mechanical resistance of the marsh scarp and by the presence of vegetation, thus limiting the response of the system to rapid variations in sea level.

References

Allen, J. R. L. (1990), Salt-marsh growth and stratification: A numerical model with special reference to the Severn Estuary, southwest Britain, *Mar. Geol.*, *95*, 77–96.

Allen, J. R. L. (2000), Morphodynamics of Holocene salt marshes: A review sketch from the Atlantic and southern North Sea coasts of Europe, *Quat. Sci. Rev.*, *19*(12), 1155–1231, doi:10.1016/S0277-3791(99)00034-7.

Amos, C. L., A. Bergamasco, G. Umgiesser, S. Cappucci, D. Cloutier, L. DeNat, M. Flindt, M. Bonardi, and S. Cristante (2004), The stability of tidal flats in Venice Lagoon—The results of in-situ measurements using two benthic, annular flames, *J. Mar. Syst.*, *51*, 211–241.

Blum, L. K., and R. Christian (2004), Belowground production and decomposition along a tidal gradient in a Virginia salt marsh, in , *The Ecogeomorphology of Tidal Marshes*, vol. *59*, edited by S. Fagherazzi, M. Marani, and L. K. Blum, pp. 47–74, AGU, Washington, D. C.

Cappucci, S., C. L. Amos, T. Hosoe, and G. Umgiesser (2004), SLIM: A numerical model to evaluate the factors controlling the evolution of intertidal mudflats in Venice Lagoon, Italy, *J. Mar. Syst.*, *51*, 257–280.

Carniello, L., A. Defina, S. Fagherazzi, and L. D'Alpaos (2005), A combined wind wave–tidal model for the Venice Lagoon, Italy, *J. Geophys. Res.*, *110*, F04007, doi:10.1029/2004JF000232.

Chapra, S. C. (1996), *Surface Water-Quality Modeling*, 784 pp., McGraw-Hill, New York.

D'Alpaos, A., S. Lanzoni, M. Marani, S. Fagherazzi, and A. Rinaldo (2005), Tidal network ontogeny: Channel initiation and early development, *J. Geophys. Res.*, *110*, F02001, doi:10.1029/2004JF000182.

D'Alpaos, A., S. Lanzoni, S. M. Mudd, and S. Fagherazzi (2006), Modeling the influence of hydroperiod and vegetation on the cross-sectional formation of tidal channels, *Estuarine Coastal Shelf Sci.*, *69*, 311–324, doi:10.1016/j.ecss.2006.05.002.

Defina, A., L. Carniello, S. Fagherazzi, and L. D'Alpaos (2007), Self-organization of shallow basins in tidal flats and salt marshes, *J. Geophys. Res.*, *112*, F03001, doi:10.1029/2006JF000550.

Einstein, H. A., and R. B. Krone (1962), Experiments to determine modes of cohesive transport in salt water, *J. Geophys. Res.*, *67*, 1451–1461.

Fagherazzi, S., and T. Sun (2003), Numerical simulations of transportational cyclic steps, *Comput. Geosci.*, *29*(9), 1143–1154, doi:10.1016/S0098-3004(03)00133-X.

Fagherazzi, S., M. Marani, and L. K. Blum (Eds.) (2004), *The Ecogeomorphology of Tidal Marshes*, *Coastal Estuarine Stud.*, vol. *59*, 266 pp., AGU, Washington, D. C.

Fagherazzi, S., L. Carniello, L. D'Alpaos, and A. Defina (2006), Critical bifurcation of shallow microtidal landforms in tidal flats and salt marshes, *Proc. Natl. Acad. Sci. U. S. A.*, *103*(22), 8337–8341, doi:10.1073/pnas.0508379103.

Fagherazzi, S., C. Palermo, M. C. Rulli, L. Carniello, and A. Defina (2007), Wind waves in shallow microtidal basins and the dynamic equilibrium of tidal flats, *J. Geophys. Res.*, *112*, F02024, doi:10.1029/2006JF000572.

Fredsoe, J., and R. Deigaard (1992), *Mechanics of Coastal Sediment Transport*, *Adv. Ser. Ocean Eng.*, vol. 3, 369 pp., World Sci., Singapore.

Kirwan, M. L., and A. B. Murray (2007), A coupled geomorphic and ecological model of tidal marsh evolution, *Proc. Natl. Acad. Sci. U. S. A.*, *104*(15), 6118–6122, doi:10.1073/pnas.0700958104.

Le Hir, P., Y. Monbet, and F. Orvain (2007), Sediment erodability in sediment transport modelling: Can we account for biota effects?, *Cont. Shelf Res.*, *27*, 1116–1142, doi:10.1016/j.csr.2005.11.016.

Möller, I. (2006), Quantifying saltmarsh vegetation and its effect on wave height dissipation: Results from a UK east coast saltmarsh, *Estuarine Coastal Shelf Sci.*, *69*, 337–351, doi:10.1016/j.ecss.2006.05.003.

Morris, J. T. (2006), Competition among marsh macrophytes by means of geomorphological displacement in the intertidal zone, *Estuarine Coastal Shelf Sci.*, *69*, 395–402, doi:10.1016/j.ecss.2006.05.025.

Morris, J. T., and B. Haskin (1990), A 5-yr record of aerial primary production and stand characteristics of *Spartina alterniflora*, *Ecology*, *71*, 2209–2217, doi:10.2307/1938633.

Morris, J. T., P. V. Sundareshwar, C. T. Nietch, B. Kjerfve, and D. R. Cahoon (2002), Responses of coastal wetlands to rising sea level, *Ecology*, *83*, 2869–2877.

Mudd, S. M., S. Fagherazzi, J. T. Morris, and D. J. Furbish (2004), Flow, sedimentation, and biomass production on a vegetated salt marsh in South Carolina: Toward a predictive model of marsh morphologic and ecologic evolution, in *The Ecogeomorphology of Tidal Marshes, Coastal Estuarine Stud.*, vol. 59, edited by S. Fagherazzi, M. Marani, and L. K. Blum, pp. 165–187, AGU, Washington, D. C.

Palmer, M. R., H. M. Nepf, T. J. R. Pettersson, and J. D. Ackerman (2004), Observations of particle capture on a cylindrical collector: Implications for particle accumulation and removal in aquatic systems, *Limnol. Oceanogr.*, *49*(1), 76–85.

Parchure, T. M., and A. J. Metha (1985), Erosion of soft cohesive sediment deposits, *J. Hydraul. Eng.*, *111*(10), 1308–1326, doi:10.1061/(ASCE)0733-9429(1985)111:10(1308).

Parker, G., M. H. Garcia, Y. Fukushima, and W. Yu (1987), Experiments on turbidity currents over an erodible bed, *J. Hydraul. Res.*, *25*(1), 123–147.

Pizzuto, J. E., and T. S. Meckelnburg (1989), Evaluation of a linear bank erosion equation, *Water Resour. Res.*, *25*(5), 1005–1013, doi:10.1029/WR025i005p01005.

Pritchard, D., A. J. Hogga, and W. Roberts (2002), Morphological modelling of intertidal mudflats: The role of cross-shore tidal currents, *Cont. Shelf Res.*, *22*, 1887–1895, doi:10.1016/S0278-4343(02)00044-4.

Randerson, P. F. (1979), A simulation of salt-marsh development and plant ecology, in *Estuarine and Coastal Land Reclamation and Water Storage*, edited by B. Knights and A. J. Phillips, pp. 48–67, Saxon House, Farnborough, U. K.

Schwimmer, R. A. (2001), Rates and processes of marsh shoreline erosion in Rehoboth Bay, Delaware, U.S.A, *J. Coastal Res.*, *17*(3), 672–683.

Schwimmer, R. A., and J. E. Pizzuto (2000), A model for the evolution of marsh shorelines, *J. Sediment. Res.*, *70*(5), 1026–1035, doi:10.1306/030400701026.

Seminara, G. (2006), Meanders, *J. Fluid Mech.*, *554*, 271–297, doi:10.1017/S0022112006008925.

Soulsby, R. L. (1997), *Dynamics of Marine Sands: A Manual for Practical Applications*, 248 pp., Thomas Telford, London.

Trenhaile, A. S. (2009), Modeling the erosion of cohesive clay coasts, *Coastal Eng.*, *56*(1), 59–72, doi:10.1016/j.coastaleng.2008.07.001.

van de Koppel, J., D. van der Wal, J. P. Bakker, and P. M. J. Herman (2005), Self-organization and vegetation collapse in salt marsh ecosystems, *Am. Nat.*, *165*(1), E1–E12, doi:10.1086/426602.

Waeles, B., P. Le Hir, and R. Silva Jacinto (2004), Modélisation morphodynamique cross-shore d'un esrtan vaseux, *C. R. Geosci.*, *336*, 1025–1033, doi:10.1016/j.crte.2004.03.011.

—————————————

S. Fagherazzi and G. Mariotti, Department of Earth Science, Boston University, Boston, MA 02215, USA. (giuliom@bu.edu)